Supporting Materials

Unraveling the effects of multi-phonon scattering mechanisms on lattice thermal conductivity of $La_2Zr_2O_7$, $La_2Sr_2AlO_7$ and $LaPO_4$ prototype thermal barrier coatings from both perturbative and non-perturbative methods based on machine learning potential

Huaxuan He [a], Xingming Wang [a], Yuzhou Hao [b], Chao Zeng [a], Jianyu Li [c], Haoliang Liu [a], Zhibin Gao[b,*], Jing Feng [c,*], Bing Xiao [a,*]

[a] State Key Laboratory of Electrical Insulation and Power Equipment, School of Electrical Engineering, Xi'an Jiaotong University, Xi'an Shaanxi, 710049, China.

[b] State Key Laboratory for Mechanical Behavior of Materials, School of Materials Science and Engineering, Xi'an Jiaotong University, Xi'an 710049, China.

[c] Faculty of Materials Science and Engineering, Kunming University of Science and Technology, Kunming, Yunnan, 650093, China.

[*] Corresponding author.

E-mail addresses: zhibin.gao@xjtu.edu.cn (Z. Gao), jingfeng@kust.edu.cn (J. Feng), bingxiao84@xjtu.edu.cn (B. Xiao).

Table S1 Default training parameters of MTP.

Parameters	Value
Radial functions	6
Radial basis size	8
Alpha moments count	2,621
Alpha index basic count	421
Alpha index times count	15,431
Alpha scalar count	500
Cutoff	5Å

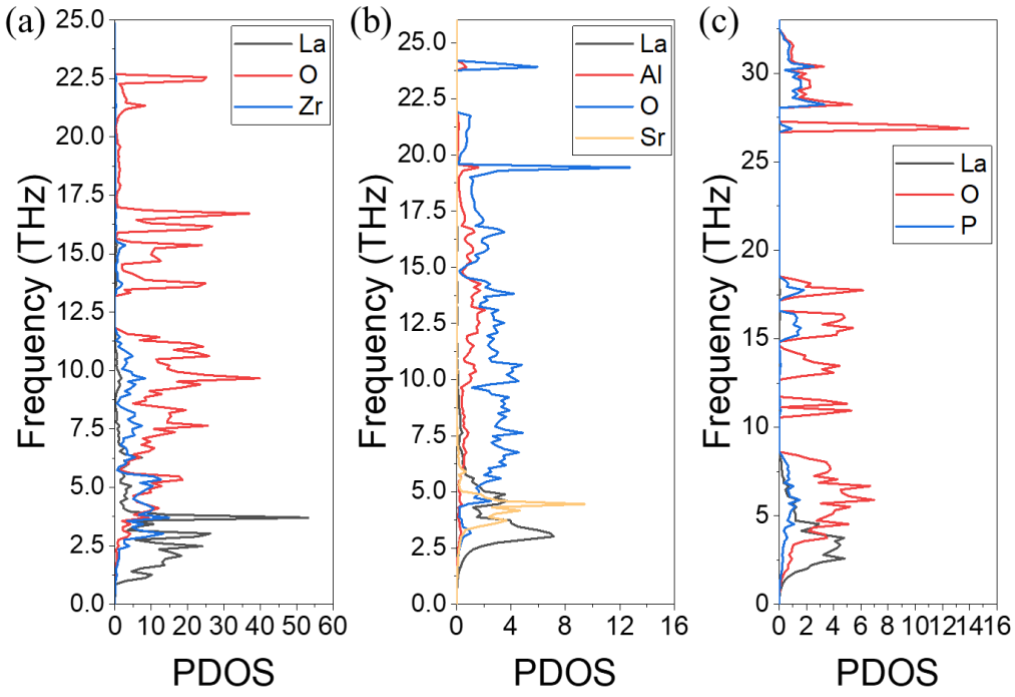

Fig. S1 PDOS obtained from temperature renormalized lattice dynamics using MTPs: (a): $La_2Zr_2O_7$; (b): $La_2SrAl_2O_7$; (c): $LaPO_4$.

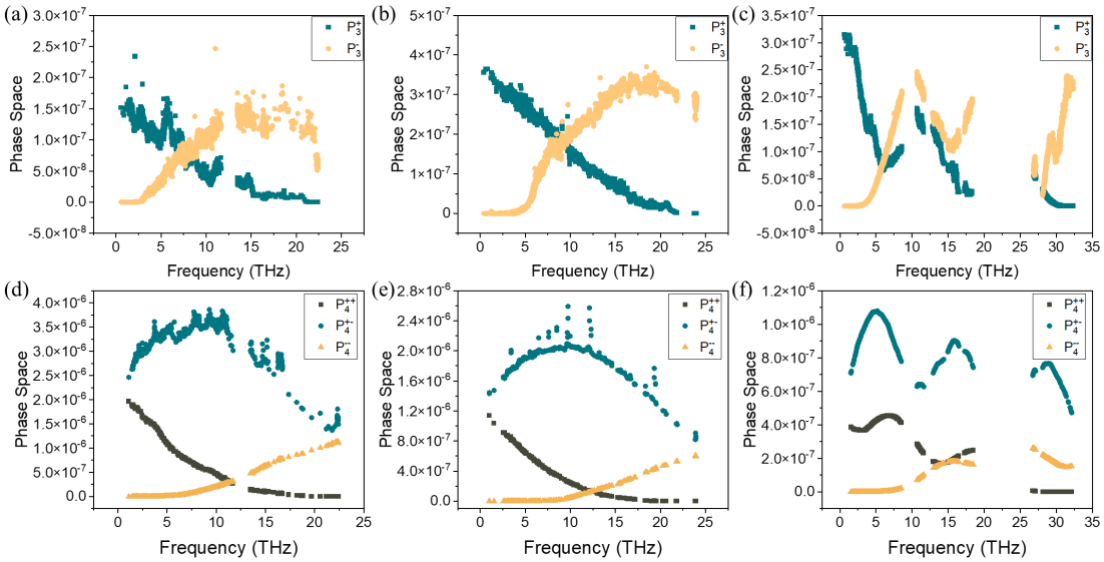

Fig. S2 The predicted multi-phonon scattering phase spaces including 3ph process on the upper panel and 4ph process of lower panel using perturbative LBTE approach at 300 K: (a) and (c): $La_2Zr_2O_7$; (b) and (d): $La_2SrAl_2O_7$; (c) and (f): $LaPO_4$.

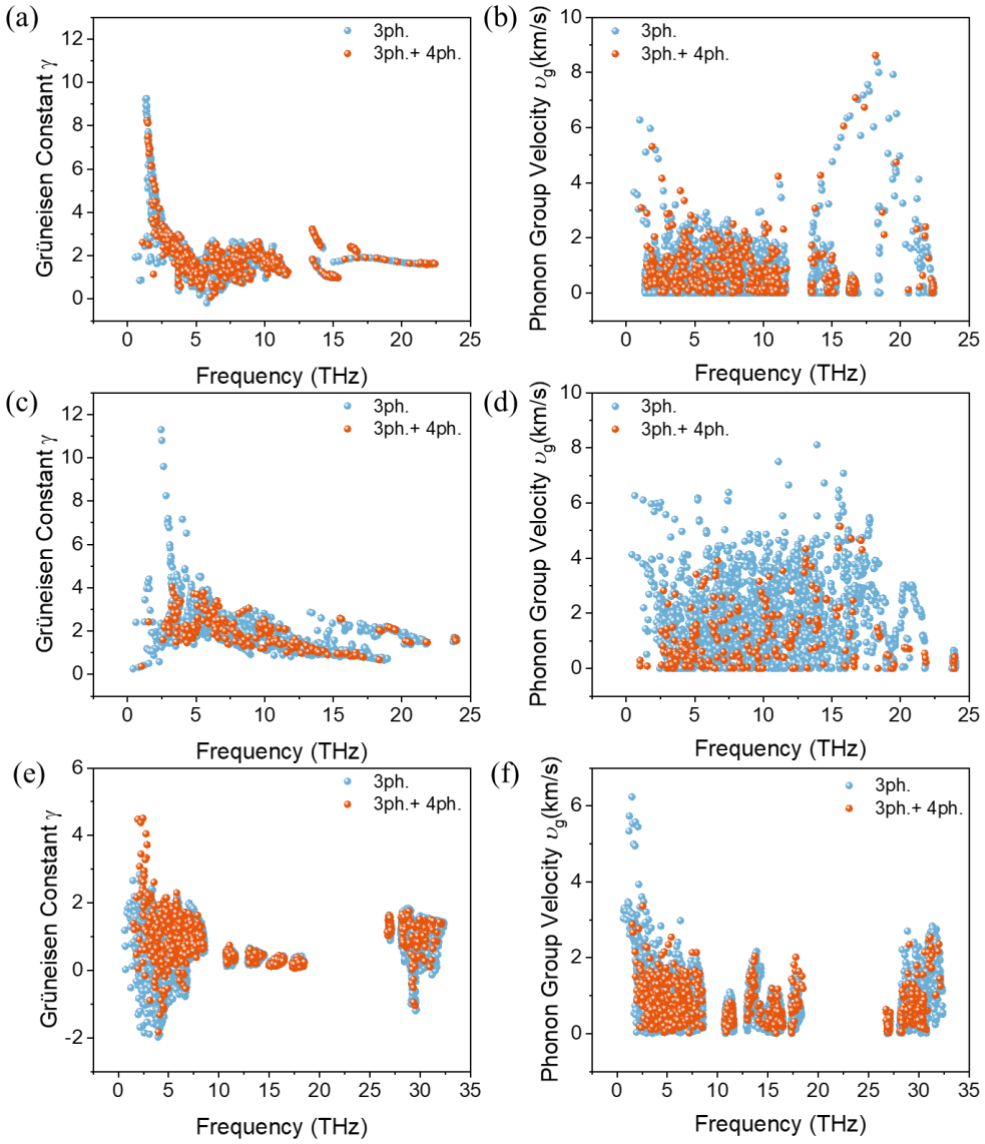

Fig. S3 Phonon model Grüneisen constants and phonon group velocity with the inclusion of three and four-phonon scattering processes for the three crystal structures within the perturbative LBTE method: (a)-(b): $La_2Zr_2O_7$; (c)-(d): $La_2SrAl_2O_7$; (e)-(f): $LaPO_4$.

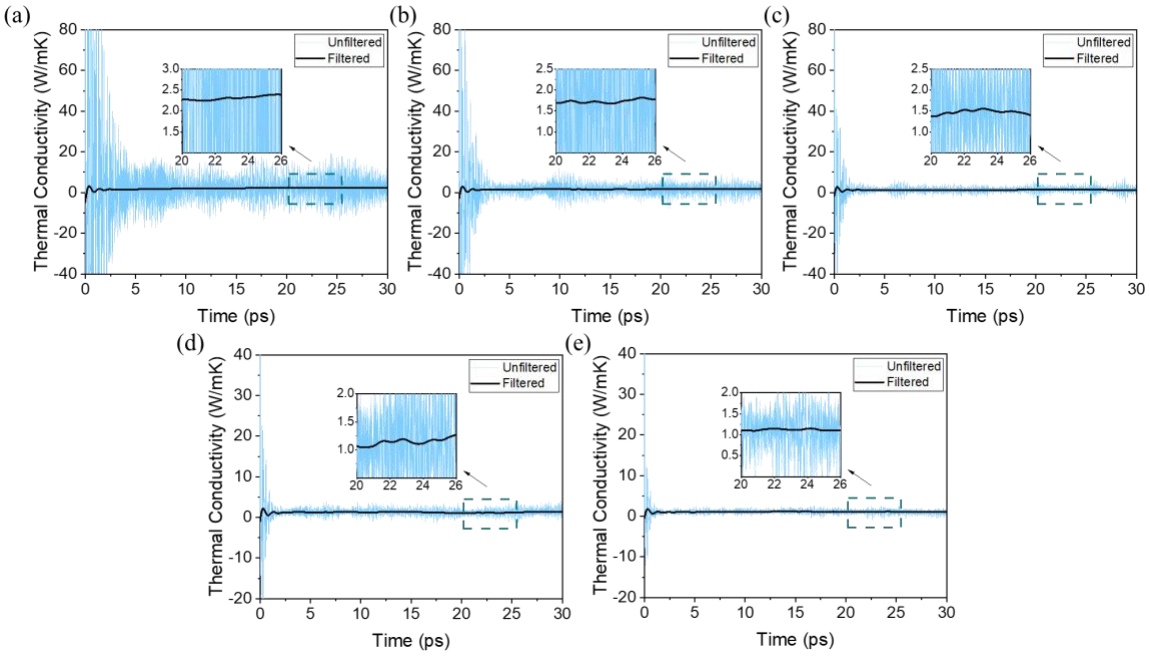

Fig. S4 Convergence behavior of lattice thermal conductivity versus correlation time in non-perturbative EMD-KG method for $La_2Zr_2O_7$: (a)300 K; (b) 500 K; (c) 800 K; (d) 1100 K; (e) 1500 K.

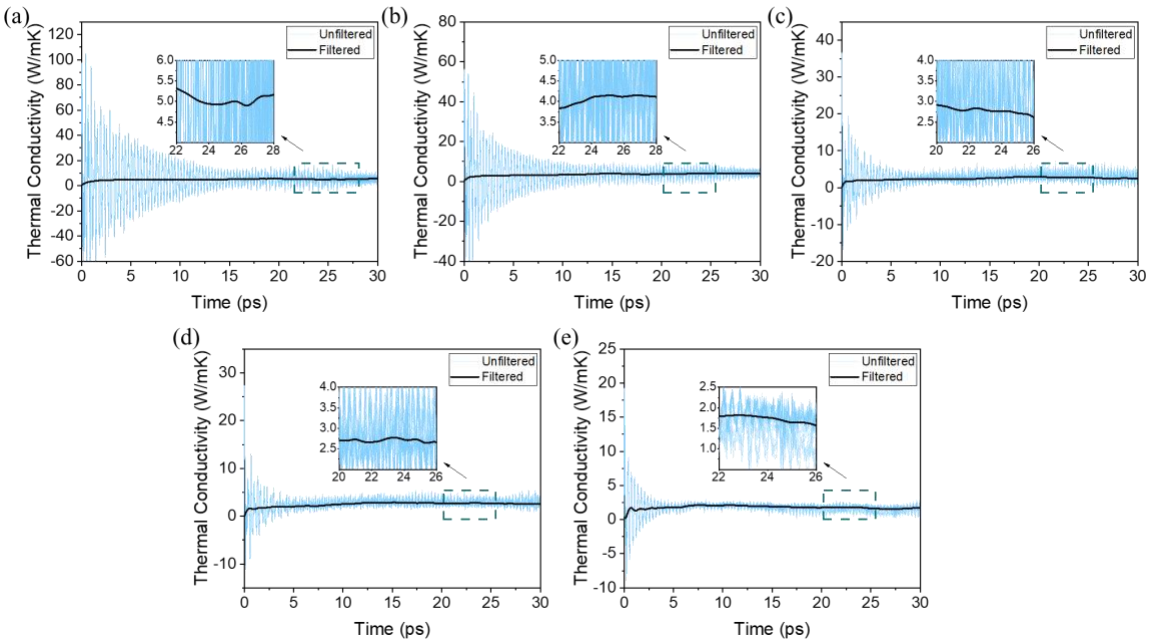

Fig. S5 Convergence behavior of lattice thermal conductivity versus correlation time in non-perturbative EMD-KG method for $La_2SrAl_2O_7$: (a)300 K; (b) 500 K; (c) 800 K; (d) 1100 K; (e) 1500 K.

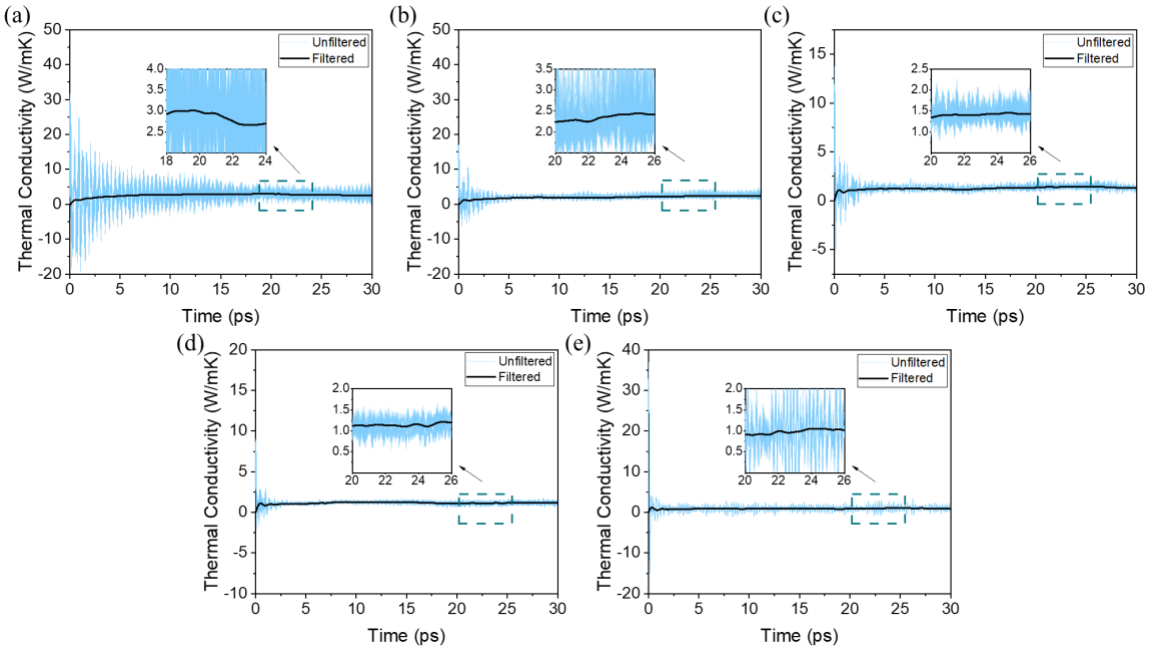

Fig. S6 Convergence behavior of lattice thermal conductivity versus correlation time in non-perturbative EMD-KG method for $LaPO_4$: (a)300K; (b) 500K; (c) 800K; (d) 1100K; (e) 1500K.

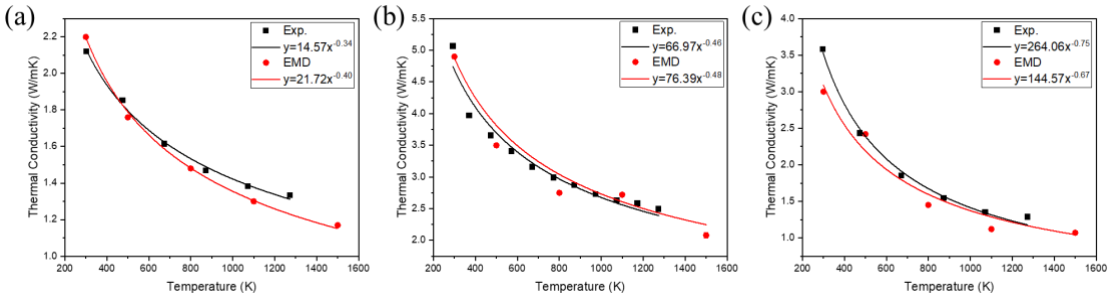

Fig. S7 Fitting curves and results of lattice thermal conductivity versus temperature for EMD and experimental values using $1/T^x$ relation: (a): $La_2Zr_2O_7$; (b): $La_2SrAl_2O_7$; (c): $LaPO_4$.

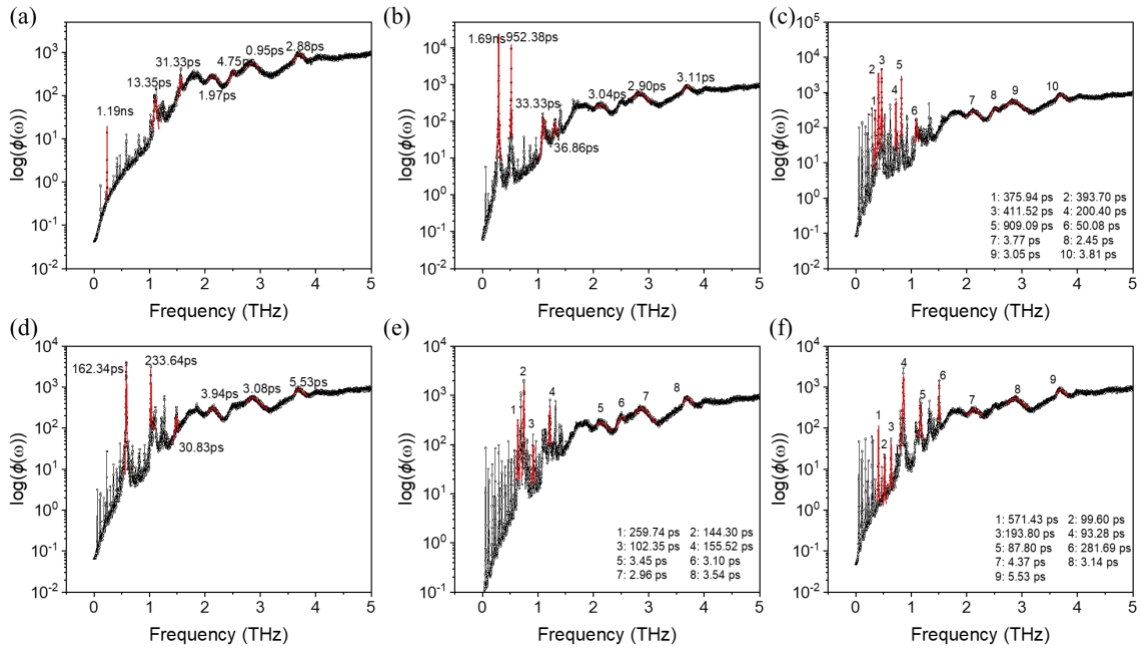

Fig. S8 All q-Slices of pSED results at 300 K and the Lorentzian fitting curves of $La_2Zr_2O_7$: (a): q = 0; (b): q = 10; (c): q = 15; (d): q = 20; (e): q = 25; (f): q = 30.

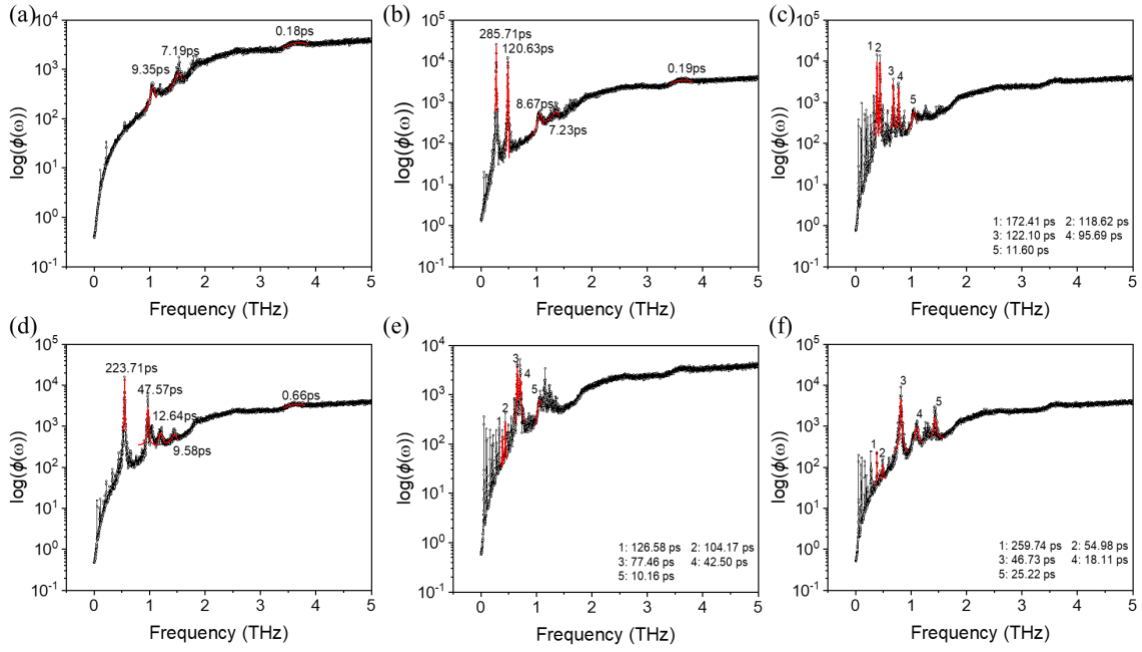

Fig. S9 All q-Slices of pSED results at 1500 K and the Lorentzian fitting curves of $La_2Zr_2O_7$: (a): q = 0; (b): q = 10; (c): q = 15; (d): q = 20; (e): q = 25; (f): q = 30.

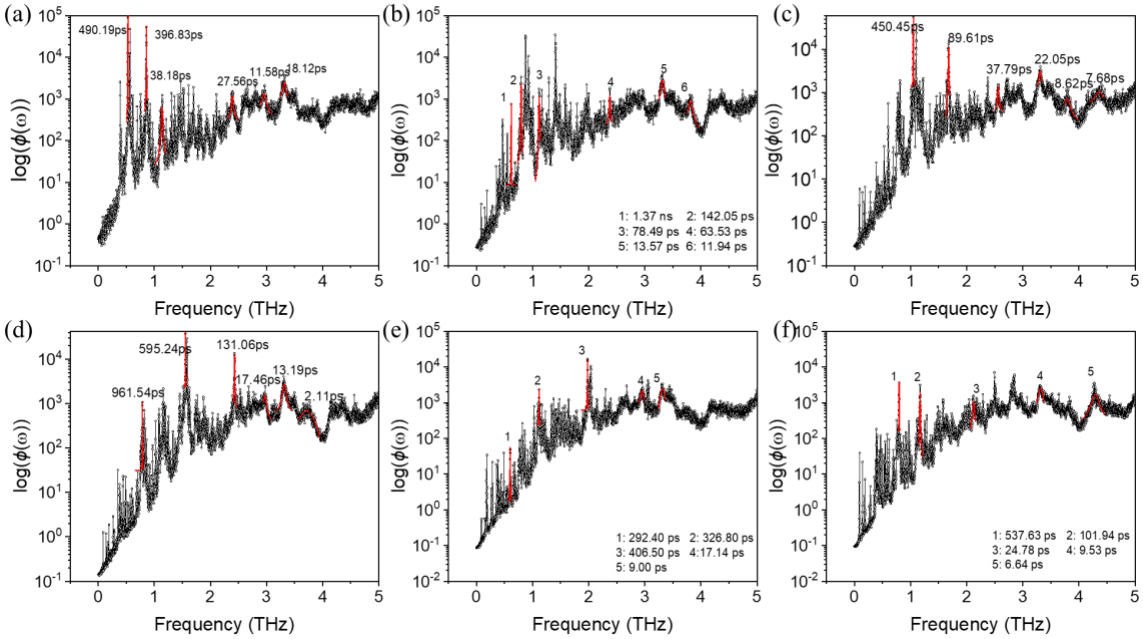

Fig. S10 All q-Slices of pSED results at 300 K and the Lorentzian fitting curves of $La_2SrAl_2O_7$: (a): q = 12; (b): q = 20; (c): q = 24; (d): q = 36; (e): q = 48; (f): q = 72.

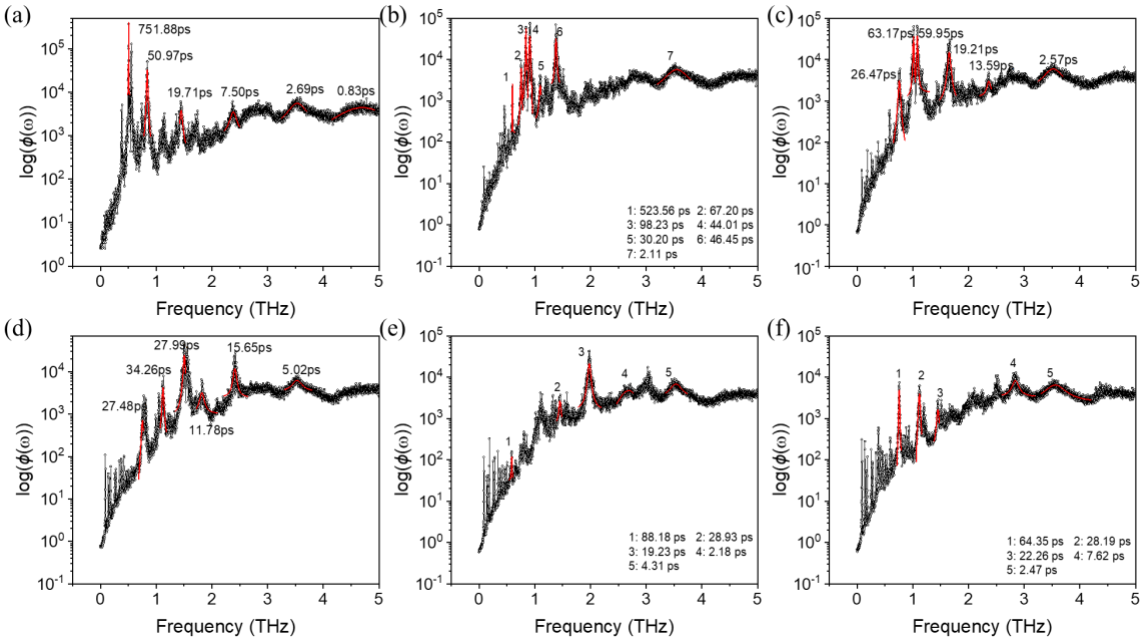

Fig. S11 All q-Slices of pSED results at 1500 K and the Lorentzian fitting curves of $La_2SrAl_2O_7$: (a): q = 12; (b): q = 20; (c): q = 24; (d): q = 36; (e): q = 48; (f): q = 72.

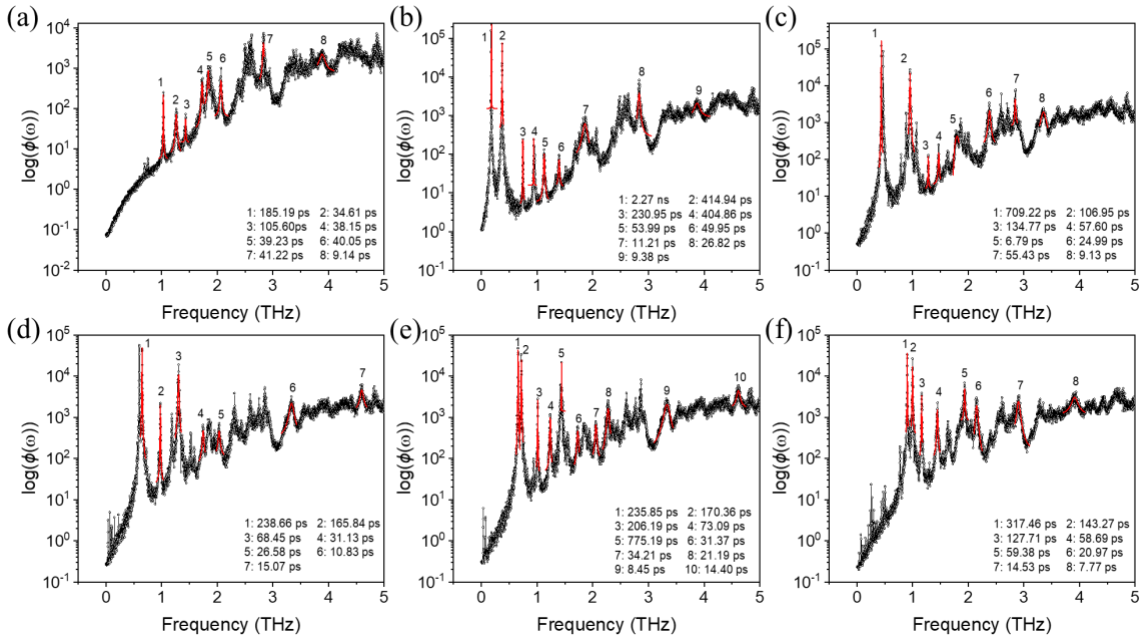

Fig. S12 All q-Slices of pSED results at 300 K and the Lorentzian fitting curves of $LaPO_4$: (a): q = 0; (b): q = 10; (c): q = 26; (d): q = 36; (e): q = 40; (f): q = 56.

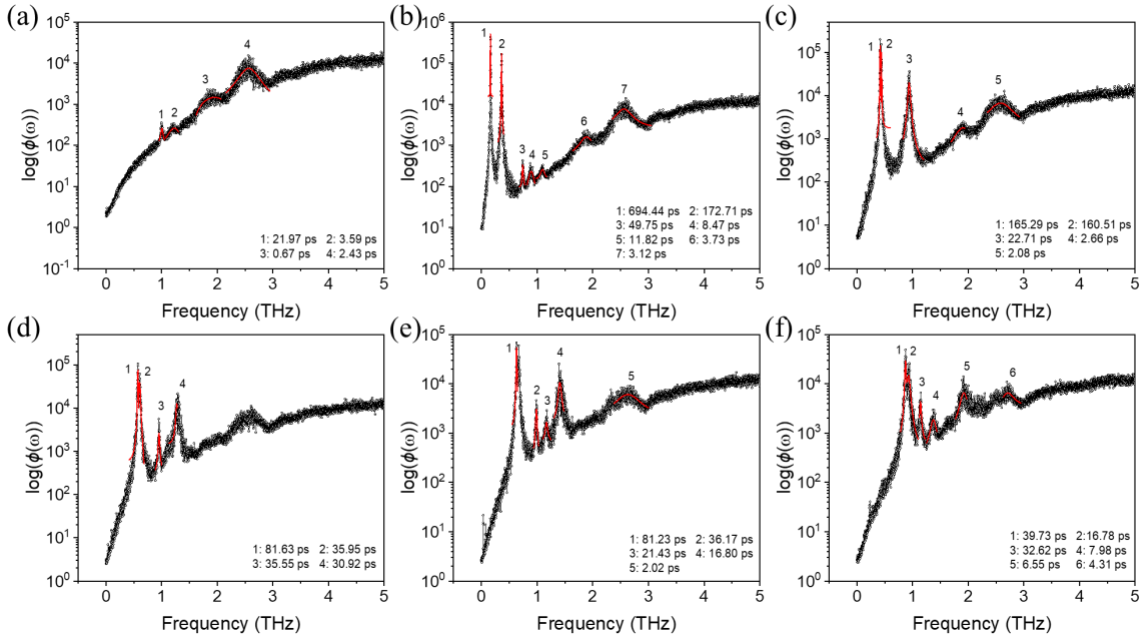

Fig. S13 All q-Slices of pSED results at 300 K and the Lorentzian fitting curves of $LaPO_4$: (a): q = 0; (b): q = 10; (c): q = 26; (d): q = 36; (e): q = 40; (f): q = 56.